Materials Today Sustainability 21 (2023) 100271

Contents lists available at ScienceDirect

Materials Today Sustainability

journal homepage: https://www.journals.elsevier.com/materials-today-sustainability

Unreported resistance in charge transport limits the photoconversion efficiency of aqueous dye-sensitised solar cells: an electrochemical impedance spectroscopy study

M. Bonomo [a, *], A.Y. Segura Zarate [a], L. Fagiolari [b], A. Damin [a], S. Galliano [a, c], C. Gerbaldi [b], F. Bella [b], C. Barolo [a, d]

[a] Department of Chemistry and NIS Interdepartmental Center and INSTM Reference Centre, University of Torino, Via Pietro Giuria 7, 10125 Torino, Italy
[b] Department of Applied Science and Technology, Politecnico di Torino, Corso Duca Degli Abruzzi 24, 10129 Torino, Italy
[c] H.Glass SA, Z.I. Du Vivier 16, CH-1690 Villaz-St-Pierre, Switzerland
[d] ICxT Interdepartmental Center, Università Degli Studi di Torino, Lungo Dora Siena 100, 10153 Torino, Italy

ARTICLE INFO

Article history:
Received 29 August 2022
Received in revised form
29 October 2022
Accepted 31 October 2022
Available online 12 November 2022

Keywords:
Water-based Electrolyte
Emerging photovoltaic
Electrolyte diffusion
Electrostatic interactions
Trap-states

ABSTRACT

In this work, a thorough electrochemical impedance spectroscopy study is performed of both liquid and polymeric aqueous dye-sensitized solar cells (a-DSSCs), which are also compared with conventional organic solvent-based devices. The main purpose is unveiling phenomena limiting the efficiency of water-based photovoltaics. Indeed, electrochemical impedance spectroscopy spectra of a-DSSCs show two peculiar (and unreported) features that are not observed in organic-based DSSCs. The higher frequency one ($R_{45°}$) is likely associated with a slowdown of the diffusion kinetics of the redox mediator: it is due to the breakdown of the hydrogen-bond network of the aqueous environment, which was also supported by density functional theory calculations. The lower-frequency feature is associated with the additional amount of energy required for the breakdown at the semiconductor/FTO interface of the adducts between protons (coming from the solvent) and electrons localized in the TiO_2 surface trap-states. This 'disruption energy' results in a resistive element (R_{IC}) that inversely correlates with the device efficiency. Very interestingly, R_{IC} depends on the applied potential and becomes negligible only at much more positive values than V_{OC}. Tailored equivalent circuits implementing simultaneously $R_{45°}$ and R_{IC} are currently under investigation.

1. Introduction

From the first report by O'Regan and Grätzel [1] in 1991, dye-sensitized solar cells (DSSCs) gathered the attention of the photovoltaic community due to their low cost and sustainability. Among the so-called emerging photovoltaics (PV), DSSCs were considered as a valid alternative to older generation Si-based devices. Actually, despite photovoltaic conversion efficiency (PCE) values are not comparable to those of conventional PV (14% *vs* 25% [2], respectively) for large-scale electricity production, they showed promising prospects of being effectively employed for building-integrated photovoltaic and indoor applications (i.e., under both low intensity and diffuse light), where the Si-based converters fail in providing good performances [3]. After continuous and progressive improvement of the performances, thanks to the development of optimized mesoporous electrodes [4] and tailored electrolytes [5], the PCE of DSSCs reached a plateau that does not seem easy to overcome [6]. At the same time, the need for stable, high-performing devices is urgent to allow commercialization and widespread market intrusion of these technologies [3]. In conventional DSSCs, limited long-term performance is mainly ascribable to the electrolyte, *viz.* a solution comprising a redox couple (generally, iodine-based) dissolved in highly volatile solvents (e.g., nitrile-based compounds like acetonitrile and 3-methoxypropionitrile), which account for corrosion and leakage issues. To address these two problems undermining the overall device stability, scientists developed innovative redox couples (based on metal complexes or organic compounds) [7] or proposed new solvents, among which water has played the main role in the last few years [8]. As a matter of fact, initially considered poisonous

* Corresponding author.
E-mail address: matteo.bonomo@unito.it (M. Bonomo).

https://doi.org/10.1016/j.mtsust.2022.100271

for DSSCs, water is now identified as a prominent component in the so-called aqueous DSSCs (a-DSSCs). Of course, to allow market competitiveness of practical-scale devices, the efficiency of a-DSSCs must be further increased at least two times to be comparable with that of the corresponding organic solvent-based counterparts. As a further improvement, the use of 100% aqueous electrolyte encompassed in a mechanically robust polymer matrix would positively impact the stability of the device, minimizing electrolyte leakage while maintaining remarkable performances [9,10]. Overall, successful development of a-DSSCs would lead to a genuinely sustainable, cheap, and safe hybrid solar cell, also compatible with portable electronics and smart textiles [11].

Amongst the DSSC-related literature reports, electrochemical impedance spectroscopy (EIS) was employed to investigate both the charge transport/recombination and diffusion phenomena taking place in a working device [12]. The so-called equivalent circuits, necessary to interpolate experimental data, were firstly developed by Bisquert and Fabregat-Santiago [13,14] for organic solvent-based cells, and they were applied, *mutatis mutandis*, to a-DSSCs. Nevertheless, compared to organic systems, the interpretation of EIS spectra is far more complex. As a matter of fact, in a-DSSCs the faster recombination process occurring at the electrode/electrolyte interface causes a convolution between EIS features, which makes the extrapolation of reliable data extremely challenging.

Herein, we report the results of a thorough EIS study of both liquid and polymeric a-DSSCs, along with a comparison with conventional organic solvent-based devices to unveil phenomena limiting the efficiency of water-based photovoltaics. In details, we focus on two peculiar features in the EIS spectra of water-based devices that are impossible to interpolate with conventional equivalent circuits, claiming further research in this direction. These contributions are related to additional resistances (with different magnitude in the case of liquid or polymeric devices) in the kinetics of both electrolyte diffusion and photoinjected electron transport, negatively impacting the photovoltaic performances of a-DSSCs. Based on our knowledge, the hereafter reported findings would be pivotal to drive the design of next-generation and efficient water-based DSSCs.

2. Materials and methods

2.1. Materials and device fabrication

NaI (99.5%, CAS: 7681-82-5), I_2 (99,8% CAS: 7553-56-2), chenodeoxycholic acid (CDCA, CAS: 474-25-9), xanthan gum (XG, from *Xanthomonas campestris*), $TiCl_4$ (99.9%, CAS: 7550-45-0), H_2PtCl_6 solution (8% in water, CAS: 16941-12-1), acetone, ethanol, acetonitrile, and *tert*-butanol were purchased from Merck and used without further purification. TiO_2 paste 18NR-T was purchased from Greatcell Solar. Milli-Q® water (18 MΩ cm at 25 °C) was obtained with a Direct-Q® 3 UV purification system (Merck Millipore). D131 was purchased from Inabata Europe SA. Surlyn 50 thermoplastic films and F-doped SnO_2 (FTO) conductive glasses (sheet resistance of 7 Ω/sq) were purchased from Solaronix. The details on electrolyte preparation and device fabrication can be found in our previous publication [18]. The dye was selected because of its molecular structure, allowing good efficiency both in aqueous and organic environments [32,33]. Briefly, in a CDCA-saturated aqueous solution, NaI and I_2 were added to obtain 3 M and 0.02 M concentrations, respectively. For gel electrolyte, 3 wt% XG was added to the previous solution and stirred overnight. The organic solvent-based electrolyte was prepared by dissolving LiI and I_2 to obtain 1 M and 0.1 M concentrations, respectively. Commercial electrolytes were avoided due to the presence of additives that are absent in homemade aqueous systems. The liquid electrolytes were introduced within the device (i.e., a D131-sensitized photoanode (0.25 cm^2) glued to a Pt-counter electrode by a Surlyn gasket) by a vacuum backfilling approach from a channel in the thermoplastic resin, that was then sealed by using a commercial epoxy glue. Conversely, in the case of hydrogel-based devices, 1.6–1.7 mg of quasi-solid electrolyte were deposited on each photoanode before the sealing process.

2.2. Device characterization

For each electrolyte type, five devices were fabricated and characterized. Errors are indicated in this manuscript using the standard deviation. Regarding photovoltaic characterization, J-V curves were recorded using a Keithley SourceMeter® kit and a VeraSol-2 LED solar simulator (class AAA, by Oriel®), calibrated with an Oriel® PV reference cell system (model 91150V). EIS spectra were recorded using an SP150 potentiostat (Bio-Logic, Inc.) under the device working condition exploiting (at V_{OC} under 1 Sun illumination) a frequency range between 100 kHz and 0.01 Hz with an amplitude of 10 mV.

2.3. Computational details

Calculations have been performed by employing the Gaussian16 code [34] and PBE [35] pure DFT-based functionals. Contributions from dispersive interactions were described through the D3-bj empirical scheme [36]. A 6-31 + G (d,p) all electrons basis set has been adopted for describing H, C, N, and O atoms. Furthermore, CRENBL effective core pseudo-potential for I^- species and the corresponding basis set (3s3p4d) were adopted [37].

In order to evaluate the energetical features of I species diffusion in water (hereafter W) and ACN, $(W)_4$ and $(ACN)_4$ tetramers organized as 4-membered rings, through which I is forced to pass, were adopted in order to simulate the above-mentioned diffusion process. The adopted models were defined starting from a central dummy atom X (placed at position P_x with x = 0.0, y = 0.0, and z = 0.0) used to define the relative positions of molecules composing the tetramers. For W and ACN, O and C_1 atoms were set as pivot ones, respectively; then, I^- species were placed and kept fixed at

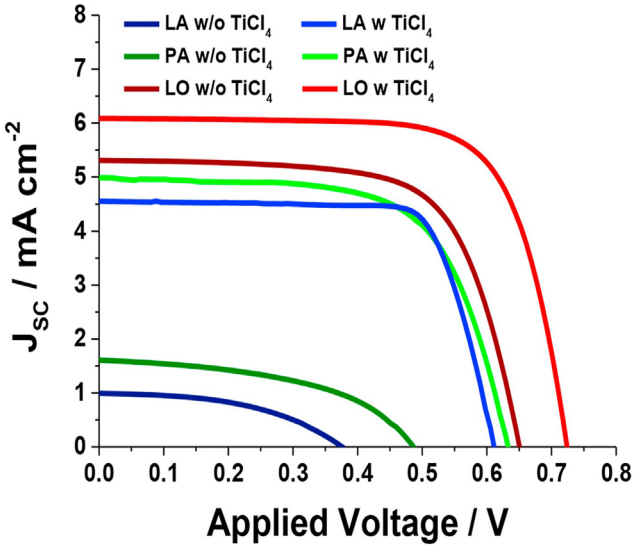

Fig. 1. J-V curves of the most efficient devices fabricated with different electrolytes: LO (in red), LA (in blue), and PA (in green). Lighter colors are referred to devices which underwent a $TiCl_4$ photoanode pre-treatment (w $TiCl_4$) whereas darker colors are referred to devices not treated (w/o $TiCl_4$).

Table 1
Averaged (n = 5) photovoltaic parameters of tested devices. FF indicates the cell fill factor.

	Ageing/h	V_{OC}/mV	J_{SC}/mA/cm^2	FF/%	PCE/%
LA w/o $TiCl_4$	24	377 ± 14	1.00 ± 0.14	47.3 ± 0.4	0.18 ± 0.04
PA w/o $TiCl_4$	24	486 ± 21	1.61 ± 0.11	48.4 ± 0.6	0.38 ± 0.08
LO w/o $TiCl_4$	24	650 ± 18	5.31 ± 0.41	67.7 ± 0.3	2.34 ± 0.14
LA w $TiCl_4$	24	627 ± 31	4.06 ± 0.21	69.7 ± 0.5	1.72 ± 0.15
PA w $TiCl_4$	24	633 ± 23	4.61 ± 0.24	70.8 ± 0.5	2.07 ± 0.15
LO w $TiCl_4$	24	723 ± 29	6.09 ± 0.25	72.4 ± 0.5	3.19 ± 0.18

several P_I (x = 0.0, y = 0.0, z = z_I; −3.0 < z_I < +3.0, Δz_I = 0.5 Å), so defining a z-direction oriented diffusion path. Finally, energetics for each new P_I value along the path was computed after a full re-optimization of all atoms (rather than the pivot ones, *vide infra*). Notice that co-planarity of pivot atoms was imposed; also, O^i-X-O^i and C_1^i-X-C_1^i angles were kept fixed at 90.0° during optimization, just O^i-X and C_1^i-X being unlocked and free to relax.

Two main quantities were considered to analyze the energetical features of I^- diffusion:

$$[\Delta E]^1 = \Delta E_{el}^{TOT} = E_{el}^{TOT}(-3.0 < z_I < 3.0) - E_{el}^{TOT}(z_I = 3.0) \quad (1)$$

where E_{el}^{TOT} refers to the electronic energy of $[I^-/(W)_4]$ and $[I^-/(ACN)_4]$ systems, respectively.

$$[\Delta E]^2 = \Delta E_{el}^{def} = E_{el}^{(W)/(ACN)_4}4(-3.0 < z_I < 3.0) - E_{el}^{(W)/(ACN)_4}4\,(z_I = 3.0) \quad (2)$$

where $E_{el}^{(W)/(ACN)_4}$ referred to the electronic energy of bare $(W)_4$ or bare $(ACN)_4$ clusters, respectively, and was kept fixed at the geometry obtained in the presence of I. For the sake of comparison, calculations for z_I = 3.0 Å and z_I = 0.0 Å were performed at B3LYP/D3-bj level too [36,38,39].

3. Results and discussion

3.1. Photovoltaic characterization of DSSCs

As stated in the introduction, EIS is likely a powerful tool to unveil the charge transfer and diffusion processes occurring in a working device. However, to be reliable, the analyzed devices should provide good performances. Therefore, we firstly characterized some devices that differ from the nature of the electrolyte (liquid organic, LO; liquid aqueous, LA; polymeric aqueous, PA) and the presence/absence of a $TiCl_4$ treatment during the preparation of the TiO_2 electrode. The latter was proven to be a valuable approach to increase the performances of the devices by slowing down the recombination reactions occurring at the sensitized photoanode/electrolyte interface [15,16]. As evidenced in Fig. 1 and Table 1, the effect of $TiCl_4$ treatment is particularly dramatic for a-DSSCs, leading to remarkably improved photovoltaic figures of merit (a 3.5-fold increase in the short-circuit current density, J_{SC}, and a 150 mV higher open-circuit voltage, V_{OC}); in the case of LO electrolyte, the effect of $TiCl_4$ is still positive but with a lower magnitude. One should note that, if untreated photoanode are employed, the use of a gelled electrolyte allows to reach higher J_{SC} and V_{OC} values following on from a partial passivation of the TiO_2 surface assured by the polymeric matrix [17]. This evidence further proved that the interfacial recombination reactions have a pivotal role in the lower PCE of water-based systems. Finally, it should be pointed out that, albeit not yet sufficiently high to be competitive with standard DSSCs, the results here proposed are comparable to the best results reported in the literature for semi-transparent DSSCs (no scattering layer) using D131 as sensitizer [18].

3.2. Electrochemical impedance spectroscopy of DSSCs

Once the photovoltaic characterization of all the devices was assessed, we proceeded with the EIS analyses of the most efficient ones. The resulting spectra of organic solvent-based systems are shown in Fig. 2a, presenting the conventional shape based on the partial convolution of three semicircles: the first (higher frequencies) being related to the charge transfer phenomenon occurring at the electrolyte/counter-electrode interface, the second one (mid frequencies) due to the charge recombination reactions (R_{rec}), taking place at the electrolyte/photoanode interface and the charge diffusion throughout the photoanode (R_t), and the third one (lower frequencies) attributed to the diffusion of the ionic species throughout the electrolyte. Following standard literature protocols, these spectra can be easily interpolated by using the so-called transmission line (TL) model (Fig. S1) developed by Bisquert *et al.* [13], which considers the mesoporous nature of the photoanode and the possible charge injection throughout the electrode thickness (i.e., statistically considering different lengths of the pathways that the injected electron should cover before reaching the conductive glass) [19].

Additionally, TL model allows to deconvolute the contribution of R_{rec} and R_t, giving a more accurate insight into the electrochemistry of the device. As a matter of fact, the most performing devices

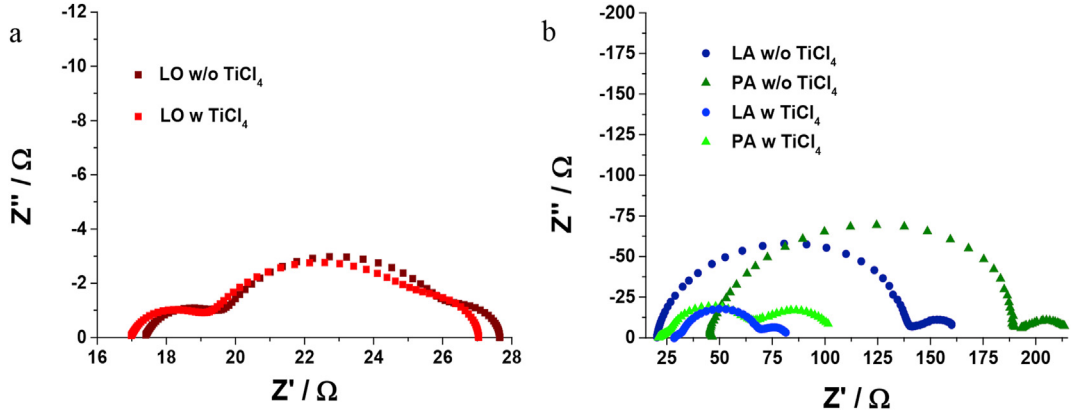

Fig. 2. Impedance spectra at V_{OC} (under 1 Sun illumination) of the most performing devices assembled with (**a**) LO electrolyte, (**b**) LA (in blue), and (c) PA (in green) electrolytes. Lighter colors are referred to device undergoing the $TiCl_4$ pre-treatment. Device area is 0.25 cm^2.

should show a low R_t/R_{rec} ratio due to the fast charge transport and the slackening of the recombination reactions: this ratio is also summarized in the electron diffusion length (L_e), that is the maximum distance an electron could travel before incurring in recombination reaction, and it is given by $L_e = l\,(R_t/R_{rec})^{1/2}$, where l is the nominal thickness of the photoanode. In this case, the $TiCl_4$ treatment led to a small - but meaningful - effect on the recombination reaction, causing a slight increase of the characteristic time for recombination (see Table 2, as extracted from the Bode plot, *vide infra*), accounting for the higher V_{OC}, J_{SC}, and PCE values reported in the previous paragraph. One should note that, with respect to R_{rec} (and values derived from it), a quantitative comparison could strictly be made only for devices experimenting similar V_{OC} values [20] (i.e., LA, PA, and LO with $TiCl_4$ and LO without $TiCl_4$). Notwithstanding this, the remarkably (roughly one order of magnitude) higher R_{rec} measured for aqueous uncoated devices, allows a reliable (yet qualitative) comparison.

If the organic electrolyte is replaced by an aqueous solution (both in the liquid and the gelled states), the analyses of EIS data become more challenging. As shown in Fig. 2b, the presence of three semicircles is only partially detectable if the photoanode is treated with $TiCl_4$; on the other hand, when no electrode treatment is carried out, the first two semicircles merge into one due to the fastening (more than one order of magnitude) of the recombination reactions, as also evidenced in the corresponding Bode plot (Fig. 3) and in accordance with previous literature reports [21,22]. One should also consider that a plausible explanation of this phenomenon could be related to the lowering of the chemical capacitance of the uncoated photoanode [23]; yet, if so, a similar behavior would be expected also in the acetonitrile (ACN)-based device (not detected in the present paper). Actually, when analyzing a-DSSCs, the efforts in the deconvolution of the EIS spectra through TL model failed; a mathematical fitting was obtained, but the errors associated with each fitted element were not acceptable. As for the previous literature reports [24,25], the most widely used equivalent circuit consists of two RC elements connected in series (Fig. S2), accounting for the electrodes/electrolyte interfaces (with the main contribution ascribable to the photoanode/electrolyte interface) and the diffusive behavior of the electrolyte, respectively. Using the latter (simplified) equivalent circuit does not allow to separate the contributions of R_t and R_{rec}, thus only partially allowing to clarify the electrochemical phenomena occurring in the working device. Moreover, such an approach could also lead to misleading results. Usually, a larger semicircle indicates a higher recombination resistance and, thus, a better photovoltaic performance; however, this inverse proportionality is only valid for systems in which the charge transport is invariant.

We tried to interpolate the experimental data with modified versions of the conventionally accepted equivalent circuits, *viz.* TL model and RC elements connected in series, but without reaching a satisfactory agreement. Other custom-made systems are currently under investigation. Albeit a proper interpolation could be obtained for the first semicircle, the description of the electrolyte diffusion does not seem to be correctly accounted.

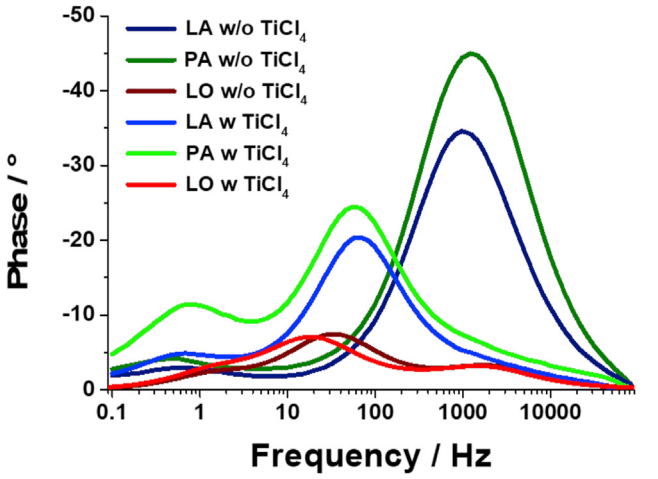

Fig. 3. Bode plot of the most performing devices fabricated with different components: LO electrolyte (in red), LA electrolyte (in blue), and PA electrolyte (in green). Lighter colors are referred to device undergoing the $TiCl_4$ pre-treatment. Device area is 0.25 cm^2.

As evidenced in Fig. S3 (highlighted with an orange line), two unusual components could be evidenced. The first one is a 45°-oriented section that usually accounts for a space-limited charge diffusion [26]. In the organic solvent-based DSSCs, such a segment is associated with the transport resistance (R_t) having a characteristic time value in the order of hundreds of μs (i.e., it is located between the high and mid frequency semicircles at the frequency of hundreds of Hz); as discussed above, a similar feature is not detectable in a-DSSCs. One could hypothesize that, following on from the replacement of ACN with water as electrolyte solvent, this segment is "'moved' toward lower frequency values. Yet, this is not feasible for two reasons: (i) if the new 45°-oriented segment would be related to charge transport phenomena throughout the TiO_2 photoanode, a dependence on the presence of a $TiCl_4$-derived coating would be expected but this is not the case (see Table 2, $R_{45°}$ column); (ii) an extremely slow charge transport time (even faster than recombination one) would imply that almost all the injected charges would recombine before being extracted at the TiO_2/TCO interface and the resulting device would not be able to produce any current.

On the other hand, the segment could be also associated to the resistance of the ionic diffusion. Indeed, it should be pointed out that ionic diffusion in DSSCs is formally modeled by exploiting a Warburg short element (W_s, finite diffusion): W_s provides a deformed arc that starts with (a short) 45° straight line at high frequencies and ends in a perfect semicircle at lower frequencies (as for the organic electrolyte) [25,27]. In the present case, we decided to proceed further with using this new notation (i.e., $R_{45°}$) to clarify that this specific contribution (more resistive than usually expected) is not simply related to the slowing down of the diffusion phenomena caused by a 'generic' increased viscosity as conventionally reported in literature [28]. Two different findings supported our choice: (i) concerning viscosity, notwithstanding the relatively higher water value (1.0 cP at 25 °C) as compared to ACN (0.33 cP at 25 °C), the calculated diffusion coefficients for I_x^- species are comparable (D_{Ix^-} = 2.1 and $1.6*10^{-5}$ cm^2/s for ACN and H_2O, respectively [29]); (ii) albeit the gelled and the liquid aqueous

Table 2
Electrochemical data extracted from the experimental EIS spectra.

	R_{rec}/Ω	R_t/Ω	t_{rec}/ms	R_{diff}/Ω	$R_{45°}/\Omega$[c]	R_{IC}/Ω[c]	PCE/%
LA w/o $TiCl_4$[a]	164.0	–	0.99	35.6	6.6	2.3	0.18
PA w/o $TiCl_4$[a]	139.7	–	0.79	40.0	8.7	2.2	0.38
LO w/o $TiCl_4$[b]	27.8	0.85	30.3	3.8	–	–	2.34
LA w $TiCl_4$[a]	39.6	–	15.3	38.0	4.4	2.0	1.70
PA w $TiCl_4$[a]	35.9	–	17.5	42.0	9.4	1.7	2.07
LO w $TiCl_4$[b]	26.9	0.66	55.9	3.6	–	–	3.19

[a] Data were interpolated by the equivalent circuit reported in Fig. S2. However, it should be clarified that the interpolated curve does not perfectly fit experimental data.
[b] Data were interpolated by the TL model equivalent circuit shown in Fig. S1.
[c] Manually calculated as |Z|. R_{diff} is the diffusion resistance experimented by the electrolyte.

systems experimented quite different viscosity, $R_{45°}$ is almost independent from the physical state of the (aqueous) electrolyte Therefore, an alternative hypothesis should be proposed: we tentatively ascribed this feature to I_x^- ion diffusion kinetics. In this context, different processes could slow down the diffusion of the anions: (i) the formation of strongly bonded ionic couples between I_x^- and positive cations (i.e., Na^+ from the salt and H^+ from water); (ii) a remarkably higher viscosity of the water-based electrolyte; (iii) the necessity to break the solvent−solvent interaction. The occurrence of ionic couples only in water is unlikely due to the very high dielectric constant ($\varepsilon_{water} = 78$ at 20 °C *vs* $\varepsilon_{ACN} = 38$), assuring an almost complete separation of the ions in solution; additionally, ionic association is expected more for Li···I (organic electrolyte) than Na···I (aqueous electrolyte), considering the larger radius of Na^+ compared to Li^+. The disruption of the solvent−solvent interaction seems to be the most likely reason behind the slowdown of the diffusion kinetics and, straightforwardly, the limitation of the photovoltaic efficiency of a-DSSCs. Indeed, establishing a hydrogen bond network within the aqueous electrolyte could resolve into an additional energy barrier to be overcome by I_x^- species in their diffusion between the electrodes. Moreover, $R_{45°}$ is almost independent from the applied voltage (*vide infra*) for both gellyfied and liquid a-DSSCs. This finding supports our hypothesis because the disruption/reconstitution of hydrogen bond networking throughout the water-based electrolytes should be (almost) independent from the application of electrical fields (simulated by the application of voltage).

Aiming at confirming such a hypothesis, calculations were performed according to the scheme described in the 'Computational details' Section. $[I(W)_4]^-$ and $[I(ACN)_4]^-$ were initially optimized keeping I species fixed at $z_I = 3.0$ Å: the analysis of Mulliken charges showed that a −1 charge was well localized on I and the analysis of the electrostatic potential distribution computed for the isolated ACN (Fig. 4, top left) and W (Fig. 4, top right) molecules well justified the obtained structures (see bottom left part of Fig. 4 for a graphical representation). The energetic features characterizing the movement of I^- in the [3.0÷-3.0 Å] z_I interval are shown in Fig. 4 (bottom right): they clearly show that I^- must overcome a significantly higher barrier to diffuse through $(W)_4$ rather than $(ACN)_4$, as well evidenced by the comparison of red ($[\Delta E]^1_W$) and dark yellow ($[\Delta E]^1_{ACN}$) solid curves: in particular, for $z_I = 0.0$, $[\Delta E]^1_W = 70.7$ kJ/mol and $[\Delta E]^1_{ACN} = 16.1$ kJ/mol. Interestingly, computation of $[\Delta E]^2_W$ and $[\Delta E]^2_{ACN}$ (dotted red and dark yellow lines in Fig. 4) at $z_I = 0.0$ resulted in 100.0 kJ/mol and 39.0 kJ/mol, respectively; this indicated a higher energetic cost for $(W)_4$ than for $(ACN)_4$ during network rearrangement needed for I^- diffusion along the selected path. Results obtained at B3LYP level substantially confirmed these findings being $[\Delta E]^1_W = 62.7$ kJ/mol and $[\Delta E]^1_{ACN} = 14.5$ kJ/mol ($[\Delta E]^2_W = 88.5$ kJ/mol and $[\Delta E]^2_{ACN} = 40.1$ kJ/mol) for $[I(W)_4]^-$ and $[I(ACN)_4]^-$, respectively.

It should be pointed out that the above-described results correlate well with the lower photovoltaic efficiency of a-DSSCs (mainly in terms of current density) than that of organic solvent-based ones, but do not explain the enhanced performance of the quasi-solid aqueous devices with respect to the liquid counterparts. Indeed, if the disruption of the solvent−solvent interaction would be the main reason for the decrease in photovoltaic efficiency, it is expected that quasi-solid devices provide lower performances.

In order to clarify this inconsistency, it is very fruitful to analyze the second unconventional feature highlighted in the EIS spectra, i.e., a straight segment parallel to the x-axis that could be ascribed to a pure resistance (i.e., the imaginary component of the

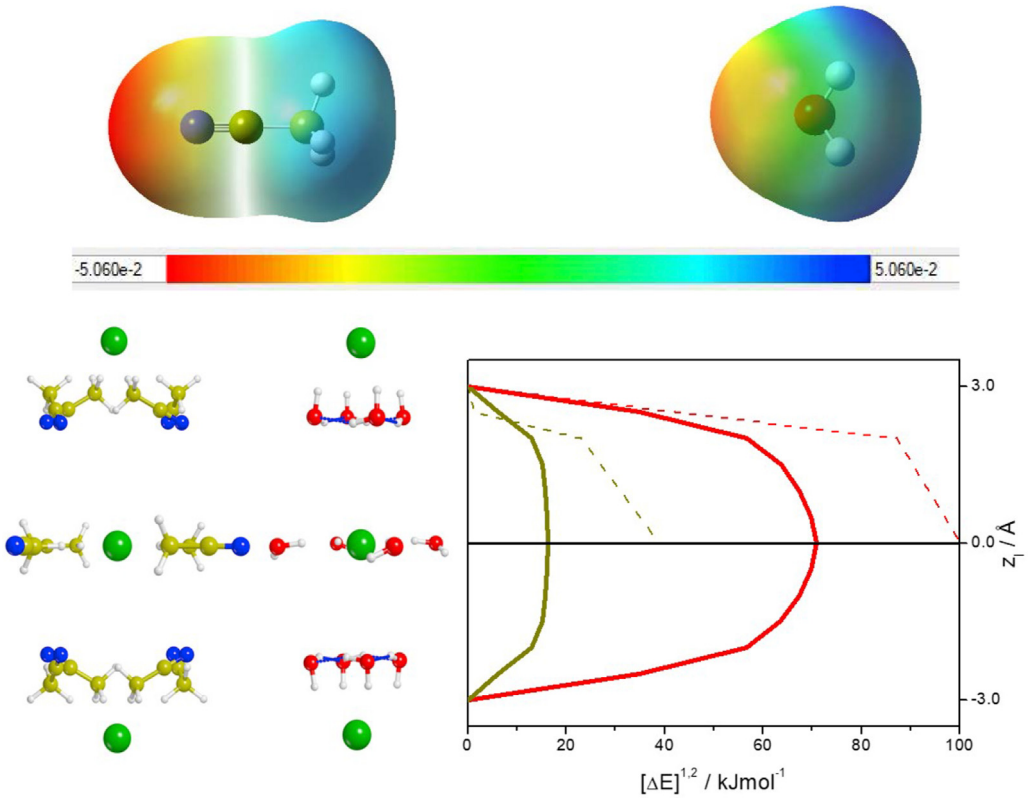

Fig. 4. Electrostatic potential maps (red and blue showing negative and positive values, respectively) computed for CH_3CN and H_2O molecules (top); graphical representation of the adopted molecular models as resulting after optimization for $z_I = 3.0$, 0.0 and −3.0 Å and $[\Delta E]^{1,2}$ plotted against z_I (bottom). Green spheres: I. Red spheres: O. Blue spheres: N. White spheres: H.

impedance is null), just before the last semicircle (highlighted with a red line in Fig. S3). To the best of our knowledge, such an element has never been reported in the EIS analyses of DSSCs. This feature could be evidenced only for water-based devices, and it is more evident (higher resistance values) when $TiCl_4$ treatment is not performed (Table 2). This prompted us to ascribe such an additional resistance to a surface-related phenomenon. As a matter of fact, when an electron is injected into the TiO_2 semiconductor, it should travel the whole electrode thickness toward the conductive glass to be extracted through the external circuit. Throughout the nanostructured TiO_2, charge transport is mainly controlled by a trapping/detrapping mechanism [30]. It should be recalled that a significant part of the photoinjected electrons are localized in the trap state, being trapping much faster than detrapping [31]. These trap states are mainly located at the semiconductor surface, originating from the lattice periodicity breakdown (e.g., dangling bonds). When an aqueous environment is conceived, these surface-localized electrons (e^-_S) could interact with protons, the concentration of which is ruled by the pH of the electrolyte (ranging between 6 and 6.5 in the present case [18]); similar interactions with alkali cations are less likely due to the higher steric hindrance of the latter, especially in an aqueous media. The claimed proton-e^-_S interaction will negatively impact the photovoltaic efficiency of a-DSSCs for two reasons: (i) the electron diffusion through the mesoporous electrode is slowed down (resulting in a higher R_t) as compared to free electrons due to the electrostatic interaction with the proton; (ii) if the latter 'follows' the e^-_S throughout the mesoporous electrode, an additional energy contribution would be necessary to break the adduct at the TiO_2/FTO interface; thus allowing an effective electron extraction. If implemented in an equivalent circuit, this additional energy will be reflected in a pure resistive element. The latter, which has been named R_{IC}, is the feature highlighted with a red line in Fig. S3.

An alternative justification of this feature could also take into account a mixed diffusion (i.e., the combination of ionic diffusion in the pores of TiO_2 with the one of the bulk electrolyte) that introduces unexpected distortion of the ideal W_s element. However, the latter explanation, even if plausible, cannot be applied in our case: indeed, diffusion through the TiO_2 pore structure should be (much) slower than the one in the bulk of the electrolyte, which in turn should result in an impedance feature at lower applied frequency (longer characteristic times). Albeit additional experimental and computational investigation are currently ongoing, the reliability of our hypothesis seems to be further proved by the

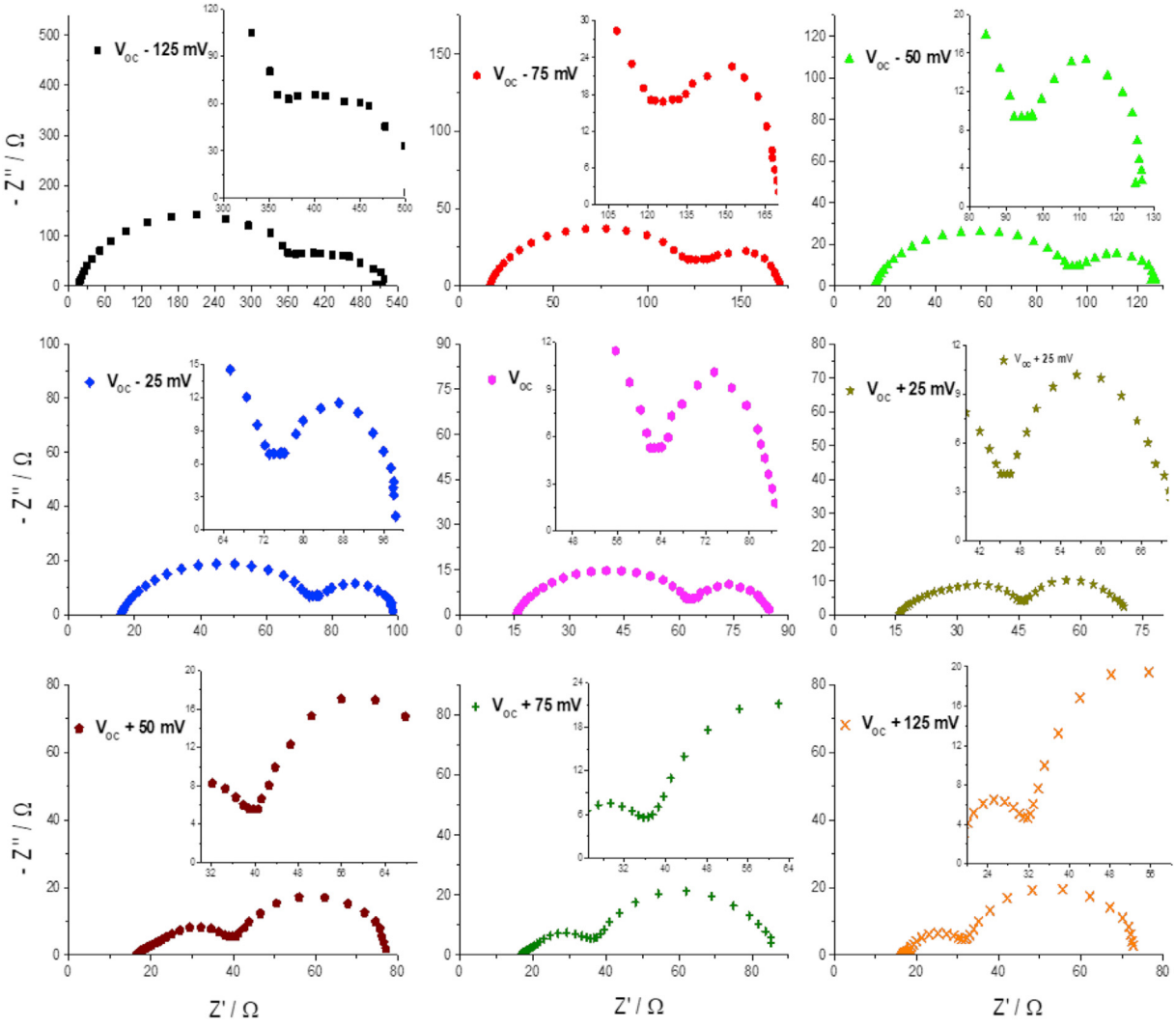

Fig. 5. Electrochemical Impedance spectra of the most performing liquid a-DSSC (LA) at different applied potential values. V_{OC} is equal to 625 mV. Area of the devices: 0.25 cm^2. In the inset, spectra zoomed in the middle-low frequency range are reported to better highlight the discussed feature, namely R_{IC}.

comparison between the EIS spectra of liquid and polymeric a-DSSCs. Indeed, the latter showed reduced R_{IC} (Table 2), likely related to the presence of the polymeric matrix that would partially passivate the photoanode surface (and thus the localized trap states), limiting the occurrence of proton-e^-_s interaction, similarly to what happened if the TiO_2 surface was modified by $TiCl_4$ treatment.

To further shed light on this unreported feature, we performed some voltage dependent EIS analyses (see Fig. 5). Applied voltage has been modulated, starting from V_{OC} to ±75 mV (with steps of 25 mV). A positive polarization ($V_{app} > V_{OC}$) promotes the charge extraction at the anode side and this counterbalances the energy required for the disruption of the proton-e^-_s adducts: the resulting R_{IC} is 1.9 Ω, 1.7 Ω, 1.2 Ω, and 0.75 Ω for $\Delta V = +25$ mV, +50 mV, +75 mV, and +125 mV, respectively (Fig. 6 and Table S1). Conversely, a negative polarization ($V_{app} < V_{OC}$) implies a lower driving force for the charge extraction leading to a higher R_{IC} value. The latter is more than doubled (i.e., 5.1 Ω) at $\Delta V = -50$ mV and it is six times higher (12.3 Ω) at $\Delta V = -75$ mV. Very interestingly, the variation of the applied potential is less dramatic when polymeric a-DSSCs are analyzed (see Fig. S4 and Table S1), perfectly matching with the passivation role of the xanthan gum matrix toward the TiO_2 surface. Therefore, the more likely formation of the above-described interactions impacts the device performances, limiting the photoconversion efficiency (mainly the J_{SC}) of LA-based devices as compared to PA counterparts. This could be related to a corrected L_e value also accounting for R_{IC} contribution. The new figure of merit, named $L_{e,eff}$, is equal to $l^*[(R_t + R_{IC})/R_{rec})]^{1/2}$ and gives the reason for the photovoltaic parameters listed in Table 1. On the other hand, $R_{45°}$ is almost independent from the applied potential (Fig. 6), especially if liquid electrolyte is employed (blue circles in Fig. 6), further confirming our hypothesis. Indeed, the diffusion of I-species will be only slightly influenced by a small variation of the applied potential (i.e., electric field).

Hereabove, we focalized our discussion on the resistive elements, whereas other fitting parameters have been showed in Tables S2–S5. Once more, R_{IC} could not be properly fitted using any of the conventionally exploited equivalent circuits. Firstly, we tested the equivalent circuit reported in Fig. S2 to interpolate experimental data, but very poor fitting could be obtained except for high applied voltages (i.e., $V_{app} > V_{OC}$ +50 mV) for both liquid and polymeric aqueous devices. As a matter of fact, at lower applied voltage, the Warburg element seems to be redundant (i.e., the experimental data were better interpolated with two R-CPE elements connected in series). One should note that the equivalent circuit reported in Fig. S2 gives good interpolation only when the R_{IC} is almost negligible (<1.5 Ω), thus further proving that the latter is a 'real' component of the impedance spectra. The latter evidence highlights the dramatic need for a tailored equivalent circuit to be designed *ex novo*.

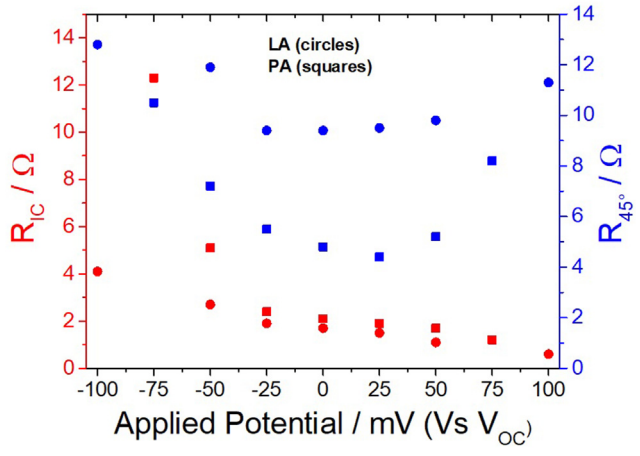

Fig. 6. Values of the resistive element R_{IC} (right axis, in red) and $R_{45°}$ (left axis, in blue) calculated from the electrochemical impedance spectra for the most performing liquid (extracted from data reported Fig. 4, here as circles) or polymeric (extracted from data reported Fig. S4, here as squares) a-DSSC measured at different applied potential values. The area of the device is 0.25 cm^2.

4. Conclusion

In the present work, we employed EIS to characterize six types of DSSCs based on organic or aqueous electrolytes (both in liquid and quasi-solid states) in which the photoanode was possibly treated with $TiCl_4$ before the sensitization procedure. In the aqueous system, the latter treatment seemed mandatory to minimize photoanode/electrolyte recombination reaction and provide good photoconversion efficiency (>2%). More importantly, we found that conventionally employed equivalent circuits are not suitable to perfectly interpolate the EIS experimental data; this is particularly evident in the low-frequency range due to the presence of two unreported features. The first, a 45°-oriented segment, was ascribed to the slowdown of the I_x^- ion diffusion kinetics related to the disruption of the hydrogen-bond network throughout the aqueous media, as also supported by density functional theory-based calculations. The second, a segment parallel to the x-axis, to the formation of proton-e^-_s, adducts that: (i) slowdown the electron transport throughout the mesoporous TiO_2 due to the electrostatic interaction, and (ii) require additional energy to be separated at the semiconductor/FTO interface (i.e., to allow the electron injection in the external circuit). The latter phenomenon led us to propose a new figure of merit ($L_{e,eff}$), accounting for both the charge transport resistance and the energy required for adduct disruption that correlates well with the device efficiency values. The results reported here point toward the need for the development of tailored equivalent circuits to interpolate EIS data of aqueous devices, as well as the further engineering of the photoanode surface and the development of tailored sensitizers to reduce the interaction of protons with photoinjected electrons. Indeed, the complete understanding of the a-DSSC (photo) electrochemistry is fundamental to develop new strategies allowing to boost device efficiency, targeting (and eventually overcoming) that of organic solvent-based counterparts.

Declaration of competing interest

The authors declare that they have no known competing financial interests or personal relationships that could have appeared to influence the work reported in this paper.

Data availability

Data will be made available on request.

Acknowledgments

This project has received fundings from the European Union's Horizon 2020 Research and Innovation Programme under grant agreement No. 826013, IMPRESSIVE. L. Fagiolari and F. Bella acknowledge funding from the European Research Council (ERC) under the European Union's Horizon 2020 Research and Innovation Programme (grant agreement no. 948769, project title SuN_2rise). This publication reflects only the author's views, and the European Union is not liable for any use that may be made of the information

contained therein. Authors kindly acknowledge Prof. M. Pavone and Prof. A.B. Munoz-Garcia for profitable discussion.

Appendix A. Supplementary data

Supplementary data to this article can be found online at https://doi.org/10.1016/j.mtsust.2022.100271.

References

[1] B. O'Regan, M. Grätzel, A low-cost, high-efficiency solar cell based on dye-sensitized colloidal TiO_2 films, Nature 353 (1991) 737–739, https://doi.org/10.1038/353737a0.

[2] NREL, Best Research-Cell Efficiency Chart | Photovoltaic Research | NREL, Best Res. Effic, Chart | Photovolt. Res. | NREL, 2022. https://www.nrel.gov/pv/cell-efficiency.html.

[3] A.B. Muñoz-García, I. Benesperi, G. Boschloo, J.J. Concepcion, J.H. Delcamp, E.A. Gibson, G.J. Meyer, M. Pavone, H. Pettersson, A. Hagfeldt, M. Freitag, Dye-sensitized solar cells strike back, Chem. Soc. Rev. 50 (2021) 12450–12550, https://doi.org/10.1039/d0cs01336f.

[4] N.A. Karim, U. Mehmood, H.F. Zahid, T. Asif, Nanostructured photoanode and counter electrode materials for efficient Dye-Sensitized Solar Cells (DSSCs), Sol. Energy 185 (2019) 165–188, https://doi.org/10.1016/j.solener.2019.04.057.

[5] H. Iftikhar, G.G. Sonai, S.G. Hashmi, A.F. Nogueira, P.D. Lund, Progress on electrolytes development in dye-sensitized solar cells, Materials 12 (2019) 1998, https://doi.org/10.3390/ma12121998.

[6] M. Kokkonen, P. Talebi, J. Zhou, S. Asgari, S.A. Soomro, F. Elsehrawy, J. Halme, S. Ahmad, A. Hagfeldt, S.G. Hashmi, Advanced research trends in dye-sensitized solar cells, J. Mater. Chem. A. 9 (2021) 10527–10545, https://doi.org/10.1039/d1ta00690h.

[7] L. Le Pleux, A.L. Smeigh, E. Gibson, Y. Pellegrin, E. Blart, G. Boschloo, A. Hagfeldt, L. Hammarström, F. Odobel, Synthesis, photophysical and photovoltaic investigations of acceptor-functionalized perylene monoimide dyes for nickel oxide p-type dye-sensitized solar cells, Energy Environ. Sci. 4 (2011) 2075–2084, https://doi.org/10.1039/c1ee01148k.

[8] F. Bella, C. Gerbaldi, C. Barolo, M. Grätzel, Aqueous dye-sensitized solar cells, Chem. Soc. Rev. 44 (2015) 3431–3473, https://doi.org/10.1039/C4CS00456F.

[9] A. Lennert, K. Wagner, R. Yunis, J.M. Pringle, D.M. Guldi, D.L. Officer, Efficient and stable solid-state dye-sensitized solar cells by the combination of phosphonium organic ionic plastic crystals with silica, ACS Appl. Mater. Interface. 10 (2018) 32271–32280, https://doi.org/10.1021/acsami.8b12334.

[10] S. Galliano, F. Bella, M. Bonomo, F. Giordano, M. Grätzel, G. Viscardi, A. Hagfeldt, C. Gerbaldi, C. Barolo, Xanthan-based hydrogel for stable and efficient quasi-solid truly aqueous dye-sensitized solar cell with cobalt mediator, Sol. RRL. 5 (2021), 2000823, https://doi.org/10.1002/solr.202000823.

[11] M. Freitag, J. Teuscher, Y. Saygili, X. Zhang, F. Giordano, P. Liska, J. Hua, S.M. Zakeeruddin, J.-E. Moser, M. Grätzel, A. Hagfeldt, Dye-sensitized solar cells for efficient power generation under ambient lighting, Nat. Photonics 11 (2017) 372–378, https://doi.org/10.1038/nphoton.2017.60.

[12] J. Villanueva-Cab, H. Wang, G. Oskam, L.M. Peter, Electron diffusion and back reaction in dye-sensitized solar cells: the effect of nonlinear recombination kinetics, J. Phys. Chem. Lett. 1 (2010) 748–751, https://doi.org/10.1021/jz1000243.

[13] F. Fabregat-Santiago, G. Garcia-Belmonte, J. Bisquert, A. Zaban, P. Salvador, Decoupling of transport, charge storage, and interfacial charge transfer in the nanocrystalline TiO2/electrolyte system by impedance methods, J. Phys. Chem. B 106 (2002) 334–339, https://doi.org/10.1021/jp0119429.

[14] F. Fabregat-Santiago, G. Garcia-Belmonte, I. Mora-Seró, J. Bisquert, I. Mora-Seroánd, J. Bisquert, Characterization of nanostructured hybrid and organic solar cells by impedance spectroscopy, Phys. Chem. Chem. Phys. 13 (2011) 9083–9118, https://doi.org/10.1039/c0cp02249g.

[15] P.M. Sommeling, B.C. O'Regan, R.R. Haswell, H.J.P. Smit, N.J. Bakker, J.J.T. Smits, J.M. Kroon, J.A.M. van Roosmalen, Influence of a TiCl 4 post-treatment on nanocrystalline TiO 2 films in dye-sensitized solar cells, J. Phys. Chem. B 110 (2006) 19191–19197, https://doi.org/10.1021/jp061346k.

[16] B.C. O'Regan, J.R. Durrant, P.M. Sommeling, N.J. Bakker, Influence of the $TiCl_4$ treatment on nanocrystalline TiO_2 films in dye-sensitized solar cells. 2. Charge density, band edge shifts, and quantification of recombination losses at short circuit, J. Phys. Chem. C 111 (2007) 14001–14010, https://doi.org/10.1021/jp073056p.

[17] G.H. Guai, Q.L. Song, Z.S. Lu, C.M. Ng, C.M. Li, Tailor and functionalize TiO_2 compact layer by acid treatment for high performance dye-sensitized solar cell and its enhancement mechanism, Renew. Energy 51 (2013) 29–35, https://doi.org/10.1016/j.renene.2012.08.078.

[18] S. Galliano, F. Bella, M. Bonomo, G. Viscardi, C. Gerbaldi, G. Boschloo, C. Barolo, Hydrogel electrolytes based on xanthan gum: green route towards stable dye-sensitized solar cells, Nanomaterials 10 (2020) 1585, https://doi.org/10.3390/nano10081585.

[19] J. Bisquert, Theory of the impedance of electron diffusion and recombination in a thin layer, J. Phys. Chem. B 106 (2002) 325, https://doi.org/10.1021/jp011941g.

[20] S.R. Raga, E.M. Barea, F. Fabregat-Santiago, Analysis of the origin of open circuit voltage in dye solar cells, J. Phys. Chem. Lett. 3 (2012) 1629–1634, https://doi.org/10.1021/jz3005464.

[21] S. Mozaffari, M.R. Nateghi, M. Borhanizarandi, Effects of water-based gel electrolyte on the charge recombination and performance of dye-sensitized solar cells, J. Solid State Electrochem. 18 (2014) 2589–2598, https://doi.org/10.1007/s10008-014-2508-x.

[22] H. Choi, C. Nahm, J. Kim, J. Moon, S. Nam, D.R. Jung, B. Park, The effect of $TiCl_4$-treated TiO_2 compact layer on the performance of dye-sensitized solar cell, Curr. Appl. Phys. 12 (2012) 737–741, https://doi.org/10.1016/j.cap.2011.10.011.

[23] F. Fabregat-Santiago, J. Bisquert, G. Garcia-Belmonte, G. Boschloo, A. Hagfeldt, Influence of electrolyte in transport and recombination in dye-sensitized solar cells studied by impedance spectroscopy, Sol. Energy Mater. Sol. Cells 87 (2005) 117–131, https://doi.org/10.1016/j.solmat.2004.07.017.

[24] H. Zhang, L. Qiu, D. Xu, W. Zhang, F. Yan, Performance enhancement for water based dye- sensitized solar cells via addition of ionic surfactants, J. Mater. Chem. A. 2 (2014) 2221–2226, https://doi.org/10.1039/c3ta14571a.

[25] S. Zhang, G.-Y.Y. Dong, B. Lin, J. Qu, N.-Y.Y. Yuan, J.-N.N. Ding, Z. Gu, Performance enhancement of aqueous dye-sensitized solar cells via introduction of a quasi-solid-state electrolyte with an inverse opal structure, Sol. Energy 127 (2016) 19–27, https://doi.org/10.1016/j.solener.2016.01.016.

[26] J. Dacuña, A. Salleo, Modeling space-charge-limited currents in organic semiconductors: extracting trap density and mobility, Phys. Rev. B - Condens. Matter Mater. Phys. 84 (2011), 195209, https://doi.org/10.1103/PhysRevB.84.195209.

[27] Q. Wang, J.-E. Moser, M. Grätzel, Electrochemical impedance spectroscopic analysis of dye-sensitized solar cells, J. Phys. Chem. B 109 (2005) 14945–14953, https://doi.org/10.1021/jp052768h.

[28] F. Fabregat-Santiago, J. Bisquert, E. Palomares, L. Otero, D. Kuang, S.M. Zakeeruddin, M. Grätzel, Correlation between photovoltaic performance and impedance spectroscopy of dye-sensitized solar cells based on ionic liquids, J. Phys. Chem. C 111 (2007) 6550–6560, https://doi.org/10.1021/jp066178a.

[29] C.L. Bentley, A.M. Bond, A.F. Hollenkamp, P.J. Mahon, J. Zhang, Voltammetric determination of the iodide/iodine formal potential and triiodide stability constant in conventional and ionic liquid media, J. Phys. Chem. C 119 (2015) 22392–22403, https://doi.org/10.1021/acs.jpcc.5b07484.

[30] A. Hagfeldt, U. Björkstén, M. Grätzel, Photocapacitance of nanocrystalline oxide semiconductor films: band-edge movement in mesoporous TiO_2 electrodes during UV illumination, J. Phys. Chem. 100 (1996) 8045–8048, https://doi.org/10.1021/jp9518567.

[31] A.C. Fisher, L.M. Peter, E.A. Ponomarev, A.B. Walker, K.G.U. Wijayantha, Intensity dependence of the back reaction and transport of electrons in dye-sensitized nanocrystalline TiO_2 solar cells, J. Phys. Chem. B 104 (2000) 949–958, https://doi.org/10.1021/jp993220b.

[32] B. Liu, Q. Liu, D. You, X. Li, Y. Naruta, W. Zhu, Molecular engineering of indoline based organic sensitizers for highly efficient dye-sensitized solar cells, J. Mater. Chem. 22 (2012) 13348–13356, https://doi.org/10.1039/c2jm31704d.

[33] Y. Wu, W.H. Zhu, S.M. Zakeeruddin, M. Grätzel, Insight into D-A-π-A structured sensitizers: a promising route to highly efficient and stable dye-sensitized solar cells, ACS Appl. Mater. Interfaces 7 (2015) 9307–9318, https://doi.org/10.1021/acsami.5b02475.

[34] M.J. Frisch, G.W. Trucks, H.B. Schlegel, G.E. Scuseria, M.A. Robb, J.R. Cheeseman, G. Scalmani, V. Barone, G.A. Petersson, H. Nakatsuji, X. Li, M. Caricato, A.V. Marenich, J. Bloino, B.G. Janesko, R. Gomperts, B. Mennucci, H.P. Hratchian, J.V. Ortiz, A.F. Izmaylov, J.L. Sonnenberg, D. Williams-Young, F. Ding, F. Lipparini, F. Egidi, J. Goings, B. Peng, A. Petrone, T. Henderson, D. Ranasinghe, V.G. Zakrzewski, J. Gao, N. Rega, G. Zheng, W. Liang, M. Hada, M. Ehara, K. Toyota, R. Fukuda, J. Hasegawa, M. Ishida, T. Nakajima, Y. Honda, O. Kitao, H. Nakai, T. Vreven, K. Throssell, J.J.A. Montgomery, J.E. Peralta, F. Ogliaro, M.J. Bearpark, J.J. Heyd, E.N. Brothers, K.N. Kudin, V.N. Staroverov, T.A. Keith, R. Kobayashi, J. Normand, K. Raghavachari, A.P. Rendell, J.C. Burant, S.S. Iyengar, J. Tomasi, M. Cossi, J.M. Millam, M. Klene, C. Adamo, R. Cammi, J.W. Ochterski, R.L. Martin, K. Morokuma, O. Farkas, J.B. Foresman, D.J. Fox, Gaussian 16, Revision A.03, Gaussian, Inc., Wallingford CT, 2016.

[35] J.P. Perdew, K. Burke, M. Ernzerhof, Erratum: generalized gradient approximation made simple (physical review letters (1996) 77 (3865)), Phys. Rev. Lett. 78 (1997) 1396, https://doi.org/10.1103/PhysRevLett.78.1396.

[36] S. Grimme, S. Ehrlich, L. Goerigk, Effect of the damping function in dispersion corrected density functional theory, J. Comput. Chem. 32 (2011) 1456–1465, https://doi.org/10.1002/jcc.21759.

[37] L.A. LaJohn, P.A. Christiansen, R.B. Ross, T. Atashroo, W.C. Ermler, Ab initio relativistic effective potentials with spin-orbit operators. III. Rb through Xe, J. Chem. Phys. 87 (1987) 2812–2824, https://doi.org/10.1063/1.453069.

[38] A.D. Becke, Density-functional thermochemistry. III. The role of exact exchange, J. Chem. Phys. 98 (1993) 5648–5652, https://doi.org/10.1063/1.464913.

[39] C. Lee, W. Yang, R.G. Parr, Development of the Colle-Salvetti correlation-energy formula into a functional of the electron density, Phys. Rev. B 37 (1988) 785–789, https://doi.org/10.1103/PhysRevB.37.785.